JCI The Journal of Clinical Investigation

Neutrophilic inflammation during lung development disrupts elastin assembly and predisposes adult mice to COPD

John T. Benjamin, … , Susan Guttentag, Timothy S. Blackwell

J Clin Invest. 2020. https://doi.org/10.1172/JCI139481.

Research In-Press Preview Inflammation Pulmonology

Graphical abstract

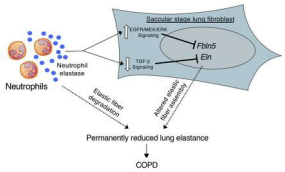

Neutrophilic Inflammation during Lung Development Disrupts Elastin Assembly and Predisposes Adult Mice to COPD

John T. Benjamin[1], Erin J. Plosa[1] , Jennifer M.S. Sucre[1,2], Riet van der Meer[1], Shivangi Dave[1], Sergey Gutor[3], David S. Nichols[3], Peter M. Gulleman[1], Christopher S. Jetter[1], Wei Han[3], Matthew Xin[3], Peter C. Dinella[1], Ashley Catanzarite[1], Seunghyi Kook[1], Kalsang Dolma[4] ,Charitharth V. Lal[4], Amit Gaggar[5,6,7], J Edwin Blalock[5,6,7], Dawn C. Newcomb[3], Bradley W. Richmond[3,8], Jonathan A. Kropski[2,3,8], Lisa R. Young[1,2,3,9], Susan H. Guttentag[1], Timothy S. Blackwell[2,3,8]

Author affiliations

[1]Department of Pediatrics, Division of Neonatology, Vanderbilt University Medical Center, Nashville, TN.

[2]Department of Cell and Developmental Biology, Vanderbilt University Medical Center, Nashville, TN.

[3]Department of Medicine, Division of Allergy, Pulmonary and Critical Care Medicine, Vanderbilt University Medical Center, Nashville, TN.

[4]Department of Pediatrics, University of Alabama at Birmingham, Birmingham, AL.

[5]Department of Medicine, Division of Pulmonary, Allergy and Critical Care, The University of Alabama at Birmingham, Birmingham, AL.

[6]Program in Protease and Matrix Biology, The University of Alabama at Birmingham, Birmingham, AL.

[7]Birmingham Veterans Affairs Medical Center, Birmingham, AL.

[8]Nashville Veterans Affairs Medical Center, Nashville, TN.

[9]Department of Pediatrics, Division of Pulmonary Medicine, Children's Hospital of Philadelphia and the Perelman School of Medicine at the University of Pennsylvania, Philadelphia, PA.

Corresponding author

John T. Benjamin M.D., MPH

Monroe Carell Jr. Children's Hopital

Vanderbilt University Medical Center

2215 B Garland Avenue, 1125C Light hall

Nashville, TN-37232

john.benjamin@vumc.org

Ph: 615-343-6495; Fax: 615-343-6182

Conflict of interest statement: The authors have declared that no conflict of interest exists.

Abstract

Emerging evidence indicates that early life events can increase the risk for developing chronic obstructive pulmonary disease (COPD). Using an inducible transgenic mouse model for NF-κB activation in the airway epithelium, we found that a brief period of inflammation during the saccular stage [postnatal day (PN)3 - PN5] but not alveolar stage (PN10 - PN12) of lung development disrupts elastic fiber assembly, resulting in permanent reduction in lung function and development of a COPD-like lung phenotype that progresses through 24 months of age. Neutrophil depletion prevented disruption of elastic fiber assembly and restored normal lung development. Mechanistic studies uncovered a role for neutrophil elastase (NE) in downregulating expression of critical elastic fiber assembly components, particularly fibulin-5 and elastin. Further, both purified human NE and NE-containing exosomes from tracheal aspirates of premature infants with lung inflammation down-regulated elastin and fibulin-5 expression by saccular stage mouse lung fibroblasts. Together, our studies define a critical developmental window for assembling the elastin scaffold in the distal lung, which is required to support lung structure and function throughout the lifespan. While neutrophils play a well-recognized role in COPD development in adults, neutrophilic inflammation may also contribute to early life predisposition to COPD.

Introduction

Although the traditional view has been that cigarette smoking causes chronic obstructive pulmonary disease (COPD) through accelerated age-related lung function decline in susceptible smokers, over the last several years it has become apparent that up to 50% of COPD may be related to reduced peak lung function in young adulthood without accelerated decline (1). In this regard, early life events have been associated with reduced adult lung function, which peaks between 20-25 years of age (2, 3). Bronchopulmonary dysplasia (BPD) is a chronic respiratory disorder of premature infants born in the saccular stage of lung development that is characterized by dilated and fewer terminal airspaces (4, 5). Several recent studies have now shown that patients with BPD have impaired lung function in adolescence and young adulthood compared to preterm infants without BPD or term infants (4, 6, 7). In addition, radiographic abnormalities, including emphysema and air trapping, have been reported on CT scans from adults with a history of BPD (8). This association between BPD and altered lung function trajectory points to the saccular stage as an important developmental window for early life events that permanently affect lung structure and function.

Data from both human studies and animal experiments indicate that inflammation in the preterm lung can alter its development (9). Infants who are exposed to chorioamnionitis in utero are likely to be born preterm and many develop BPD (10). Similarly, infections in the early postnatal period increase BPD risk in premature infants (11). Previously, we reported that perinatal transgene activation in mice engineered to express an inducible form of IKKβ, the upstream activator of the master inflammatory transcription factor NF-κB, in airway epithelial cells results in early postnatal death with hypoxemia, dilation of terminal saccules, and disorganized elastic fiber formation (12). Based on these findings, we hypothesized that transient

NF-κB-induced inflammation during the saccular stage of lung development could disrupt formation of the elastin scaffold of the distal lung, resulting in permanently impaired lung function. Therefore, we modified this model to induce sublethal inflammation and injury during either the saccular (PN3-PN5) or alveolar stage (PN10-PN12) of mouse lung development. Remarkably, epithelial-derived inflammation in the saccular, but not alveolar, stage resulted in an early BPD-like phenotype with disruption of the developing elastin meshwork in the distal lung, followed by emphysematous airspace dilation with reduced lung function that persisted through 24 months of age. These studies define a critical window in saccular stage lung development for establishing the elastin scaffold required to support distal lung structure and function throughout the lifespan.

Results

NF-κB activation in the saccular stage results in permanent abnormalities in lung structure and function.

In mice with doxycycline (Dox)-inducible expression of constitutively active human IκB-kinase β (IKKβ) in airway epithelium (called IKTA mice) (13), we induced transient transgene expression in pups during lung development by treating lactating dams with Dox in drinking water from postnatal day (PN)3 – PN5 (saccular) or PN10 – PN12 (alveolar). We then examined lungs of IKTA and litter-mate control mice over time. At 2 months of age, lungs of adult IKTA mice with Dox administration from PN3 – PN5 showed marked emphysematous changes throughout the lung parenchyma (Figure 1, A and B). In contrast, lungs of adult IKTA mice with Dox from PN10 – PN12 appeared similar to control lungs on histological evaluation. In addition, small airways from IKTA mice with PN3 – PN5 Dox exhibited a significant reduction in the number of radial alveolar attachments (Figure 1, C and D), which are connective tissue-containing septa that insert radially into the adventitia of small airways and are responsible for tethering to adjacent alveolar tissue (14).

We next evaluated elastic fibers in the lungs of 2 month-old IKTA mice and found that elastic fibers were fragmented and reduced in number throughout the lung parenchyma of 2 month-old IKTA mice with Dox administration from PN3 – PN5, while 2 month-old IKTA mice with Dox from PN10 – PN12 demonstrated normal cord-like arrangement of elastic fibers around distal airspaces, similar to those seen in littermate controls (Figure 1E). Together, these data suggest that brief periods of NF-κB-induced inflammation during saccular stage lung development disrupts assembly of the elastic fiber scaffold, resulting in long-term pathological alterations in the distal lung parenchyma.

As elastic fibers have a very long half-life and as their assembly is developmentally regulated (15, 16), we followed IKTA mice (Dox PN3 – PN5) to 24 months of age to investigate the life-long consequences of saccular stage lung inflammation. At 24 months, elderly IKTA mice (Dox PN3 – PN5) had a striking emphysematous phenotype that was visible at the time of lung harvest and on lung sections, along with persistent elastic fiber fragmentation and disorganization (Figure 2, A-C). Flow cytometry for immune cells and mRNA expression of inflammatory cytokines revealed no evidence of ongoing inflammation in IKTA mice (Dox PN3-PN5) at 3 or 24 months of age compared to controls (Supplemental Figure 1), thereby suggesting that progressive emphysematous changes in these mice did not result from persistent lung inflammation.

To evaluate the trajectory of structural changes in the lung parenchyma of IKTA mice with saccular stage transgene activation, we performed morphometric evaluation of lungs from IKTA mice (Dox PN3 – PN5) and littermate controls at 2, 6, and 24 months of age. As shown in Figure 2D and E, progressive alveolar enlargement [measured by mean linear intercept (MLI)] and reduction in alveolar attachment counts were identified from 2 to 24 months of age in littermate control mice, demonstrating the effects of aging; however, IKTA mice (Dox PN3 – PN5) had increased MLI and reduced alveolar attachments at each time-point compared to controls. Collectively, these findings indicate that impaired elastic fiber organization during saccular lung development permanently alters lung structure and, with the effects of aging, results in progressive worsening of emphysema and alveolar attachment loss.

To investigate the functional consequences of altered lung structure in IKTA mice (Dox PN3 – PN5), we measured lung mechanics by FlexiVent (SCIREQ, Montreal, Qubec). Compared to littermate controls and IKTA mice with transgene activation during the alveolar

stage (Dox PN10 – PN12), 2 month-old IKTA mice with Dox from PN3 – PN5 had reduced lung elastance, reduced respiratory system elastance, and increased lung compliance (Supplemental Figure 2). As mice aged from 2-24 months, elastance decreased and compliance increased in control mice, but IKTA mice (Dox PN3 – PN5) had reduced lung tissue elastance and respiratory system elastance, along with increased compliance, at each timepoint compared to littermate controls (Figure 2, F-H). As an additional control group, we evaluated untreated IKTA mice (never exposed to Dox) at 24 months of age and found that lung histology was identical to littermate controls (Supplemental Figure 3A). Also, compared to both littermate controls and non-Dox treated IKTA mice, 24 month-old IKTA mice (Dox PN3 – PN5) had reduced lung tissue elastance, reduced respiratory system elastance, increased lung compliance, and increased inspiratory capacity (Supplemental Figure 3, B - E). Thus, alterations in lung function mirror progression of emphysematous changes in lungs of IKTA mice subjected to saccular stage lung inflammation.

Transgene activation in IKTA mice results in neutrophilic inflammation during the saccular and alveolar stages of lung development, but elastin fiber assembly is impaired only during the saccular stage

To investigate the short-term effects of transgene activation in IKTA mice during lung development, dams were placed on Dox in drinking water from PN3 – PN5 (saccular stage) or PN10 – PN12 (alveolar stage) and lungs were examined at PN5 or PN12, respectively. As expected, transgene expression was detected in IKTA lungs at PN5 and PN12 (Figure 3A). IKTA lungs at both time points showed a neutrophil predominant inflammatory cell influx (Figure 3, B and C). Consistent with the inflammatory cell influx at PN5 and PN12, expression of

inflammatory cytokines was robustly induced in Dox-treated IKTA lungs at both PN5 and PN12 compared to controls (Figure 3, D and E).

At PN5, abnormal lung development with dilated airspaces and aberrant organization of elastic fibers was apparent in IKTA mice (Dox PN3 – PN5) (Figure 4, A - C). Impaired elastic fiber assembly correlated with reduced mRNA expression of elastin (*Eln*) and fibulin-5 (*Fbln5*), but not other critical components of elastic fiber assembly in PN5 IKTA lungs (Figure 4D and Supplemental Figure 4A). In contrast, lung development was not altered at PN12 in IKTA mice with Dox from PN10 – PN12 (Figure 4, E and F). Both elastic fiber organization and expression of *Eln*, *Fbln5* and other critical components of elastic fiber assembly were similar between PN12 control and IKTA lungs (Figure 4, G and H and Supplemental Figure 4B). Collectively, these data show that neutrophilic inflammation selectively down-regulates expression of *Fbln5* and *Eln* and alters elastic fiber organization in saccular stage lungs.

As parenchymal growth in the saccular lung is closely related to vascular growth around distal airspaces (17), we examined whether vasculogenesis was altered in IKTA mice (Dox PN3 – PN5). Immunostaining for von Willebrand's Factor, an endothelial cell marker, in PN5 lungs revealed no differences in vessel density between Dox-treated control and IKTA lungs. Expression of the angiogenic growth factor *Vegfa* and its primary receptor *Flk1* (Vegfr2) were also similar between Dox-treated control and IKTA lungs at PN5 (Supplemental Figure 5, A and B). In addition, immunostaining for α-smooth muscle actin (α-SMA) showed well-organized smooth muscle cells around large vessels in both control and IKTA lungs, along with intact elastic lamina (Supplemental Figure 5, C and D). These findings indicate that inflammation-induced changes in IKTA lungs primarily affect structural support for developing saccules, without impairment of vasculogenesis.

Since saccular stage transgene activation resulted in a profound developmental phenotype in IKTA mice, we wondered whether lung inflammation during this timeframe altered proliferation or survival of parenchymal cell populations in the developing lung. Evaluation of proliferating cell nuclear antigen (PCNA) positive cells in PN5 (Dox PN3 – PN5) control and IKTA lung sections revealed no differences in proliferation of type 2 alveolar epithelial cells or other parenchymal cells in Dox-treated IKTA compared to control lungs (Supplemental Figure 6, A - C). We also performed TUNEL staining of PN5 control and IKTA lung sections and found similar numbers of TUNEL+ cells in both groups (Supplemental Figure 6D). Thus, altered lung development in IKTA mice does not appear to result from major shifts in proliferation or survival of non-immune cell populations.

Neutrophil depletion rescues lung development in mice with saccular stage inflammation

Since neutrophils predominated in the inflammatory phenotype of saccular stage IKTA mice, we administered anti-Ly6G antibodies (or control IgG) to IKTA and littermate control mice by intraperitoneal (IP) injection on PN2 in order to block the neutrophil influx induced by Dox treatment from PN3-PN5. Flow cytometry analysis (Figure 5, A and B) and immunostaining for Gr-1 (Supplemental Figure 7) confirmed reduced neutrophil recruitment in Dox-treated IKTA lungs at PN5 following administration of anti-Ly6G antibodies.

Neutrophil depletion normalized lung development in IKTA mice (Dox PN3 – PN5), while control IgG had no effect on the BPD-like phenotype (Figure 5, C - E). To test whether neutrophil depletion corrects long-term lung development in IKTA mice (Dox PN3 – PN5), these mice were injected with anti-Ly6G antibodies on PN2 and evaluated at the completion of lung development (PN30). At this timepoint, neutrophil depleted IKTA mice showed normal alveolar

structure (Supplemental Figure 8), further supporting the conclusion that neutrophils mediate aberrant lung development in this model.

Next, we investigated whether neutrophils were responsible for down-regulation of *Eln* and *Fbln5* expression in saccular stage lungs from IKTA mice (Dox PN3 – PN5). As shown in Figure 6A, anti-Ly6G antibody treatment mitigated down-regulation of these elastic fiber assembly components in PN5 IKTA lungs. In situ hybridization (RNAscope) confirmed the reduction in *Fbln5* and *Eln* in PN5 IKTA lungs and restoration of expression following anti-Ly6G antibody treatment (Figure 6B). Consistent with these findings, neutrophil depletion corrected the fragmented and disorganized appearance of elastic fibers around saccular airspaces of PN5 IKTA mice (Figure 6C).

As elastic fiber assembly components are primarily produced by mesenchymal cells in the developing lung, we tested whether IKTA neutrophils could directly alter mRNA expression of elastic fiber assembly components by these cells. For these experiments, we used fluorescent activated cell sorting (FACS) to isolate $CD45^+/CD11b^+/Ly6G^+$ neutrophils from IKTA lungs (Dox PN3 – PN5) and then co-cultured these cells with wild-type primary saccular stage mouse (PN5) lung fibroblasts. IKTA neutrophils down-regulated *Fbln5* and *Eln* expression by saccular lung fibroblasts (Figure 6, D and E), suggesting that recruited neutrophils (or their soluble mediators) are responsible for the altered elastic fiber assembly observed in inflamed saccular stage lungs.

Neutrophil-derived cytokines do not inhibit elastin assembly

Having identified neutrophils as the primary immune cell type responsible for disrupting elastic fiber assembly in saccular stage IKTA lungs, we investigated molecular mechanisms by which neutrophils could mediate these effects. While expression of a variety of inflammatory

cytokines was increased in IKTA lungs (Dox PN3 – PN5), only IL-1β expression was altered by neutrophil depletion (Supplemental Figure 9A). Since IL-1β signaling has been shown to alter saccular stage lung development (18), we tested whether exogenous IL-1β could affect elastin and fibulin-5 expression in cultured saccular stage mouse lung fibroblasts (Supplemental Figure 9B). Since these data suggested that IL-1 signaling could be responsible for the deleterious effects of neutrophils in saccular stage IKTA lungs, we generated IKTA mice deficient in IL-1R1, the primary IL-1 signaling receptor; however, IL-1R1 deletion did not rescue the saccular lung phenotype in IKTA mice (Dox PN3 – PN5) (Supplemental Figure 9, C - E) and did not prevent the down-regulation of *Eln* and *Fbln5* in IKTA lungs (Supplemental Figure 9F).

Neutrophil elastase down-regulates mRNA expression of elastic fiber assembly components by saccular stage lung fibroblasts

Since neutrophil elastase (NE) was increased in IKTA lungs after Dox treatment (Figure 7A and Supplemental Figure 10A), we wondered whether NE mediates the BPD-like phenotype in PN5 IKTA mice. Therefore, we co-cultured lung neutrophils ($CD45^+/CD11b^+/Ly6G^+$ cells) obtained by flow sorting from IKTA lungs with wild-type saccular stage mouse lung fibroblasts in the presence or absence of an irreversible NE inhibitor (N-Methoxysuccinyl-Ala-Ala-Pro-Val-chloromethyl ketone). Treatment with the NE inhibitor normalized expression of *Eln* and *Fbln5* by fibroblasts co-cultured with IKTA neutrophils (Figure 7B). Further, addition of purified human neutrophil elastase (HNE) to culture media down-regulated *Eln* and *Fbln5* expression by saccular stage lung fibroblasts (Figure 7C). In comparison, HNE treatment did not affect expression of *Eln* and *Fbln* in cultured PN12 (alveolar stage) lung fibroblasts (Supplemental Figure 10B), suggesting developmental stage-dependent regulation of mRNA expression for these elastin assembly genes.

NE is increased in airways of patients with BPD (19, 20) and recent data suggest that exosomes harvested from tracheal aspirates of BPD patients express active NE on their surface (21). Therefore, we tested whether BPD exosomes could down-regulate elastic fiber assembly components by saccular stage lung fibroblasts. For these experiments, we collected tracheal aspirate exosomes from preterm patients with BPD (or term-born controls) (Supplemental Table 1) and treated saccular stage mouse lung fibroblasts with pooled exosomes from BPD or control patients. BPD exosomes had higher neutrophil elastase activity (BPD - 0.9 μg of HNE equivalent activity/10^{10} exosomes; control - 0.06 μg of HNE equivalent activity/10^{10} exosomes) and down-regulated fibroblast *Eln* and *Fbln5* (Figure 7, D and E), thus implicating NE-containing exosomes in blocking production of critical elastic fiber assembly components.

Based on our finding that NE suppresses expression of elastin assembly components in addition to degrading elastin, we tested whether saccular stage lungs are uniquely susceptible to NE exposure compared to lungs during later stages of development (alveolarization) or after completion of lung development (adults). For these studies, we generated precision cut lung slices (PCLS) from PN5, PN12, and adult (2 month-old) wild-type mice, and cultured each PCLS with or without HNE (4 μg/ml) for 4 days. HNE treatment resulted in airspace dilation of PN5 PCLS with marked reduction of intact elastic fibers (Supplemental Figure 11). In contrast, at this concentration and exposure time, HNE treatment of PN12 or adult PCLS did not alter alveolar architecture and elastin fibers remained intact, thereby supporting the conclusion that saccular stage lungs are uniquely susceptible to the damaging effects of NE.

Neutrophil elastase activates the EGFR-MEK-ERK pathway and inhibits TGF-β signaling in saccular stage lung fibroblasts

To investigate the mechanisms by which NE regulates transcription of critical elastic fiber assembly components in mesenchymal cells, we first tested several candidate pathways that have previously been shown to be activated by NE and/or down-regulate elastin assembly components, including Par-1, Par-2, NF-κB and p38 MAPK (22-25). Using specific inhibitors of each of these pathways in conjunction with NE treatment of PN5 fibroblasts, we found no impact on NE-mediated suppression of *Eln* or *Fbln5* expression (Supplemental Figure 12).

Elastases can cleave membrane bound pro-forms of epidermal growth factor receptor (EGFR) ligands, including TGF-α, EGF and heparin-binding EGF (HB-EGF), and release active ligands that trans-activate EGFR (26-29). Therefore, we measured EGFR ligands in culture media from PN5 fibroblasts after HNE treatment and found that EGF and Hb-EGF were undetectable, but TGF-α was increased by 15 minutes, suggesting proteolytic release (Figure 8A). We then treated saccular stage lung fibroblasts with recombinant TGF-α and found that expression of *Fbln5* and *Eln* was reduced (Figure 8, B and C), thereby indicating that HNE-mediated release of TGF-α could down-regulate *Fbln5 and Eln* expression. To further investigate whether EGFR signaling mediates the effects of HNE on *Fbln5* and *Eln* expression, we treated PN5 fibroblasts with HNE and the selective EGFR tyrosine kinase inhibitor AG1478. As shown in Figure 8D, EGFR inhibition prevented *Fbln5* (but not *Eln*) down-regulation. Since mitogen-activated protein kinase kinase (MEK)/extracellular signal-regulated kinase (ERK) signaling can be induced by EGFR activation, we measured ERK phosphorylation after HNE treatment and found increased ERK phosphorylation by 15 minutes after treatment (Figure 8, E and F). We then treated PN5 fibroblasts with the MEK/ERK inhibitor U0126 along with HNE and found that the MEK/ERK inhibitor prevented *Fbln5* down-regulation but did not affect *Eln* expression, similar to EGFR inhibition (Figure 8G). Together, these data show that NE treatment

activates EGFR-MEK-ERK signaling to inhibit *Fbln5* expression in saccular stage fibroblasts; however, additional pathways are involved in *Eln* regulation.

To further investigate the mechanisms by which NE suppresses *Eln* expression in saccular stage lung fibroblasts, we examined the TGF-β pathway, which has been reported to regulate *Eln* expression in human and neonatal rat lung fibroblasts (28, 30). Consistent with prior reports, we found that TGF-β neutralizing antibodies and the TGF-β receptor kinase inhibitor SB431542 reduced *Eln* expression and exogenous TGF-β1 treatment up-regulated *Eln* expression in PN5 lung fibroblasts (Supplemental Figure 13, A and B). To test whether NE-dependent suppression of *Eln* expression could be mediated by inhibition of canonical TGF-β signaling, PN5 lung fibroblasts were transfected with a Smad2/3 luciferase reporter plasmid prior to HNE treatment. HNE treatment reduced reporter activity in both control and TGF-β1 stimulated cells (Figure 9, A and B), along with down-regulation of TGF-β regulated genes, including *Ctgf*, *Serpine-1* and *Tbsp1* (Figure 9C). We then pretreated PN5 lung fibroblasts with TGF-β1 prior to HNE treatment and found that addition of TGF-β1 prevented HNE-induced down-regulation of *Eln* expression and modestly increased *Fbln5* expression (Figure 9, D and E). Collectively, these data suggest that interruption of canonical TGF-β signaling in saccular lung fibroblasts by HNE is important for down-regulation of *Eln* expression.

Discussion

Our studies identify a window of susceptibility in the saccular stage of lung development (embryonic day 18 – PN5 in mice, 23 – 34 weeks gestation in humans) during which neutrophilic inflammation can disrupt formation of the elastic fiber network in the distal lung leading to lifelong impairment in lung structure and function. The saccular stage marks a critical period during development in which the preterm lung undergoes numerous changes required for successful transition to postnatal life, including production and assembly of nascent elastic fibers in the extracellular matrix surrounding developing saccules. Neutrophilic inflammation, which could occur as a result of infection (chorioamnionitis) or injury to the developing lung, prevents normal assembly of elastic fibers around terminal airspaces and leads to BPD-like alveolar simplification, followed by a sustained reduction in lung function with airspace enlargement (emphysema) and loss of alveolar attachments surrounding small airways that progresses with advancing age. This phenotype is at least partially driven by NE, which has a dual role of down-regulating expression of key elastin assembly components, particularly *Fbln5* and *Eln*, as well as matrix destruction.

As lung function trajectories appear to be established early in childhood (2, 31), injuries that reduce lung function during early life could limit the peak lung function attainable in adulthood; thereby representing a major risk factor for COPD (2, 32). This idea is supported by multiple studies showing that extremely preterm human infants who develop BPD continue to have lung function abnormalities during their growing years (4-6, 33, 34). In addition to prematurity, maternal smoking, childhood lower respiratory infections, malnutrition, and air pollution may also contribute to the low lung function phenotype in adulthood (35, 36). Therefore, while the saccular stage of lung development appears to be uniquely susceptible to neutrophilic

inflammation, other insults during alveolarization and lung growth may also alter lung function trajectory. An important question for future studies is whether subtle inflammatory insults during the saccular stage, which are insufficient to cause BPD, can instigate enough disruption in elastin fiber assembly to restrict peak lung function and predispose to COPD.

Neutrophils have been implicated as an important cell type in COPD pathogenesis for many years. The "protease/anti-protease hypothesis" for COPD development is based on the phenotype seen in smokers with alpha-1 antiprotease deficiency, in which continued lung inflammation results in an imbalance of matrix degrading enzymes (particularly NE), favoring destruction of gas exchanging units and accelerated decline in lung function (37, 38). It was unexpected, however, that neutrophils could also play a critical role in early life predisposition to COPD through a separate function of inhibiting elastin assembly. Our studies show that impaired elastin fiber assembly around developing saccules leads to emphysematous airspace dilation and a reduction in alveolar attachments surrounding distal airways, both of which affect elastic recoil and could contribute to airflow limitation. Although the effects of emphysema on lung function are well-known, the loss of alveolar attachments and their contribution to airflow limitation in COPD are under-appreciated (39, 40). Reduction in alveolar attachments is thought to untether small airways from adjacent alveolar tissue, thereby contributing to dynamic airflow limitation through reduced radial tension and premature closure of small airways during expiration (14, 41).

Neutrophils are critical mediators of innate immune signaling in the lung and can contribute to inflammatory lung injury in both the neonatal and adult lung (42-44). For example, neutrophils mediate alveolar simplification in neonatal rats exposed to hyperoxia (45). In adult IKTA mice, treatment with Dox drives robust transgene activation and a neutrophil-predominant

inflammatory cell influx, resulting in acute lung injury with substantial mortality beginning around day 7 of transgene inducton (13). Longer term treatment with low-dose Dox causes a COPD-like phenotype in IKTA mice with emphysema, elastin degradation, and small airway wall remodeling by 3-4 months of treatment (46). In our studies, neutrophil depletion rescued the saccular stage lung phenotype in IKTA mice, thus confirming neutrophils as the culprit for mediating the effects of inflammation on elastic fiber assembly. While it is tautology that NE can cleave elastin and other components of the lung extracellular matrix, more recent studies indicate that NE can also modulate gene expression (26, 47, 48). Depending on the cell type and context of signaling, NE may either up-regulate (47, 48) or down-regulate gene expression (28, 49). In saccular, but not alveolar, stage mouse lung fibroblasts, we found that NE suppresses expression of *Eln* and *Fbln5*, thus suggesting the possibility that distinct subpopulations of fibroblasts (with differential susceptibility to NE) produce elastin and elastin assembly components in the saccular and alveolar stage. While this issue requires further investigation, our findings indicate that mesenchymal cells in the saccular stage lung are particularly susceptible to NE.

Since exosomes harvested from tracheal aspirates of infants with BPD contain active NE on their surface and administration of these exosomes can induce a BPD-like phenotype in mice (21), we tested whether BPD exosomes could affect expression of elastin assembly components by saccular stage fibroblasts. In keeping with a dual function of NE in saccular stage lung development, we found that BPD patient exosomes inhibited *Eln* and *Fbln5* expression by saccular stage lung fibroblasts. Collectively, these findings build on prior work demonstrating succeptibility of elastin organization in the saccular stage lung to inflammation (12), and highlight what we believe to be a novel role for NE in dysregulating elastic fiber assembly in the saccular lung mesenchyme.

In our studies, we showed that downregulation of *Fbln5* by NE in saccular stage lung fibroblasts is mediated through the EGFR-MEK-ERK signaling pathway. EGFR signaling is important for early lung morphogenesis (50) and reduced EGFR signaling increases apoptosis and prevents lung growth in newborn mice exposed to mechanical ventilation with hyperoxia (51). However, aberrant EGFR activation can also be detrimental to the neonatal lung (52) and EGFR ligands, including EGF and TGF-α, are increased in lungs of infants with BPD (52, 53). In this regard, transgenic over-expression of human TGF-α in the early postnatal mouse lung alters elastic fiber organization and lung structures leading to COPD-like changes in the adult lung, similar to those seen in IKTA mice with transgene activation during the saccular stage (54). Although previous studies have shown that neutrophil elastase can cleave cell membrane bound pro-forms of EGFR ligands, including EGF, HB-EGF and TGF-α (26-29), we found that only TGF-α (but not EGF or HB-EGF) was increased in conditioned media from NE-treated PN5 lung fibroblasts, suggesting a likely role for soluble TGF-α in activating EGFR in NE-treated saccular stage lung fibroblasts. However, given the complexity of the in vivo setting, other EGFR ligands or non-ligand mediated activation of EGFR, could also play a role in *Fbln5* down-regulation in lungs of IKTA mice.

In contrast to *Fbln5, Eln* expression by saccular stage lung fibroblasts appears to be primarily regulated by pathways other than EGFR, particularly the TGF-β pathway (30, 55). Prior reports indicate that autocrine TGF-β signaling can increase fibroblast *Eln* expression by stabilizing *Eln* mRNA (56). We found that HNE downregulates autocrine TGF-β dependent Smad signaling in PN5 fibroblasts, and addition of exogenous TGF-β restored *Eln* expression after HNE treatment. Although full elucidation of mechanisms connecting NE and intracellular signaling pathways in saccular stage lung fibroblasts requires additional study, NE appears to

alter a variety of signaling pathways in fibroblasts, including EGFR-MEK-ERK and TGF-β, which can perturb elastin assembly and alter lung development during the saccular stage.

Although our studies specifically focused on the role of NE, we acknowledge that other neutrophil products may also affect the abnormal saccular stage lung phenotype that we observed in IKTA mice. IL-1β is increased in the lungs of preterm infants at risk for chronic lung disease (57, 58) and transgenic expression of human IL-1β in the mouse lung alters saccular stage lung development (18). In the hyperoxia model of BPD, abrogating IL-1β-mediated IL-1R1 signaling prevents abnormalities in saccular stage lung development (59). Although neutrophils are an important source of IL-1β, genetic deficiency of IL-1R1 in our *in vivo* studies did not prevent abnormalities in elastin assembly or rescue the abnormal saccular stage lung phenotype that we observed in lungs of IKTA mice. Thus, specific molecular mechanisms contributing to impaired lung development may depend on the context and type of inflammatory stimulus.

In summary, our findings delineate the saccular stage as a critical period for laying down the elastic fiber scaffold in the lung. NE secreted by activated neutrophils down-regulates production of critical elastic fiber assembly components and alters assembly of elastic fibers in the saccular stage, thereby resulting in persistent deficits in lung function and a COPD-like adult lung phenotype. These findings may have relevance in understanding the developmental origins of COPD and other adult lung diseases.

Methods

Mouse models

All mice used for experiments in this study were on a C57BL/6 background. Transgenic mice that express a FLAG-tagged form of activated human IKKβ containing S177E and S188E mutations under the control of a tetracycline operator minimal CMV promoter and a tetracycline-controlled transcription silencer under the control of the Clara cell 10 kDa (CC10) promoter have been previously described (FLAG-IKKβ mice) (13). To activate NF-κB in the airway epithelium, hemizygous FLAG-IKKβ male mice were crossed with homozygous female mice expressing reverse tetracycline transactivator (rtTA) under control of the Club cell specific protein promoter (CCSP-rtTA mice) . Approximately half of the pups from these matings expressed all three transgenes and activated NF-κB in the airway epithelium after treatment with doxycycline (Dox). These mice were designated IKTA mice, and the remaining pups in each litter that expressed only the CCSP-rtTA transgene were used as littermate controls. For transgene activation in neonatal lungs, lactating dams were administered 100 mg/L of Dox (Sigma-Aldrich) in drinking water from PN3 – PN5 (saccular stage transgene activation) or from PN10 - PN12 (alveolar stage transgene activation). In some experiments, IKTA mice deficient in IL-1R1 were also used. IL-1R1 -/- mice (B6.129S7-*Ilr1* ^{tm1Imx}/J – Stock number- 003245) were purchased from Jackson laboratories. FLAG- IKKβ and CC10-rtTA mice were separately backcrossed to IL-1R1 -/- mice to generate FLAG-IKKβ and CCSP-rtTA mice deficient in IL-1R1 respectively. IL-1R1 -/- FLAG- IKKβ and IL1R1 -/- CCSP-rtTA mice were then crossed to generate IKTA mice (and litter-mate controls) deficient in IL-1R1.

To block neutrophil influx, neonatal IKTA mice (and litter-mate controls) were administered a neutralizing anti-Ly6G antibody (20 μg of antibody per pup, Clone 1A8, Cat #

BP0075-1, Bio X Cell) or an IgG1a isotype control antibody (20 µg of antibody per pup, Cat # BP0089, Bio X Cell) intraperitoneally (IP) on PN2, prior to Dox administration from PN3-PN5. Lungs were then harvested on PN5 for additional studies.

Lung function measurements

After transgene activation from PN3 – PN5 or from PN10 - PN12, IKTA and litter-mate control mice were serially followed and lung function measurements were quantified at various time-points using the FlexiVent apparatus (SCIREQ, Montreal, Qubec) and established methods (60, 61). Briefly, mice were anesthetized with pentobarbital sodium (85 mg/kg) and an 18-guage tracheostomy tube was placed in the trachea. Mice were then mechanically ventilated using the SCIREQ FlexiVent apparatus with 150 breaths/min and a tidal volume of 10 ml/kg body weight prior to lung function measurements. Respiratory system elastance and compliance was captured using the Flexivent "Snapshot model" and tissue elastance (H) was captured using constant phase model to obtain a parametric distinction between airway and tissue mechanics.

Precision Cut Lung Slices

Precision cut lung slices (PCLS) were made from neonatal mouse lungs at PN5 or PN12 or from adult mouse lungs using previously published methods (62, 63). Briefly, after euthanasia, lungs were perfused with cold phosphate buffered saline after which a blunt-tipped catheter was inserted into the trachea. Low melting temperature agarose (2 % agarose in DMEM: F12 -1:1) was then instilled into the lung via the tracheal catheter, following which the lung was removed *en bloc* and placed on ice. Two hundred fifty micrometer thickness sections were cut from the left lobe using a Leica VT1000E vibrating microtome tissue slicer (Leica Biosystems). Tissue slices were cultured in DMEM: F12 with or without human neutrophil elastase treatment

for up to 96 hours at 37ºC after which lung slices were harvested and fixed in 10% formalin for additional studies.

Flow cytometry

Lung tissue was digested using Collagenase XI (Sigma-Aldrich- C7657 0.7 mg/ml), type IV DNase (Sigma-Aldrich – D5025 30 ug/ml) and Dispase (0.25 mg/ml) and filtered through a 70 μm filter to obtain a single cell suspension. Cells were labelled with conjugated primary antibodies and analyzed using a 3-laser BD Fortessa analytical flow cytometer (BD Biosciences) and FlowJo software (BD Biosciences). Conjugated primary antibodies used for flow cytometry were as follows: CD45-BV510 (clone 30-F11; BioLegend), CD11b- PE-Cy7(clone M1/70; BioLegend), Ly6G-APC-Cy7 (clone 1A8; BioLegend), CD64-APC (clone X54-5/7.1; Biolegend), F4/80-PE-Cy5 (clone BM8, Biolegend), Siglec F-PE (clone E50-2440; BD Pharmingen), Ly6C-PerCP-Cy5.5 (clone AL-21; BD Pharmingen) and I-A/I-E MHC-II-FITC (clone 2G9; BD Pharmingen). DAPI (Sigma-Aldrich) labelling was used to assess cell viability.

To isolate saccular lung neutrophils, PN5 lung tissue was first digested and processed to a single cell suspension as above. Cells were then labelled with conjugated primary antibodies and subjected to florescence activated cells sorting on a FACSAria ll cell sorter (BD Biosciences) with FACSDiVa v6.1 software (BD Biosciences) to isolate CD45 + CD11b + Ly-6G + neutrophils that were collected for in vitro experiments.

Histology and immunostaining

Whole mouse lungs and neonatal mouse PCLS were fixed overnight with 10% formalin prior to paraffin embedding and staining sections with hematoxylin and eosin (H&E) using standard methods. Images of H&E sections were then imaged using a brightfield microscope. For immunoperoxidase staining, after rehydration and antigen retrieval using citrated buffer-pH

6.5, 5 μm paraffin sections were sequentially incubated with primary and biotinylated secondary antibodies. Immunostaining was then detected using ABC kits and NovaRED reagents (Vector Laboratories). Slides were counterstained with hematoxylin prior to imaging using a brightfield microscope. For immunofluorescent staining, lung sections were first permeabilized with 0.1% Triton X-100 (Thermo Fisher Scientific). Then, after overnight incubation with primary antibodies, sections were incubated with Alexa-conjugated secondary antibodies as indicated and imaged using a fluorescent microscope. Elastic fibers were localized in lung sections using Hart's elastin stain using previously described methods (12).

Morphometry and image analysis

For morphometric evaluations, brightfield images of H&E stained lung sections were captured as TIFF files and imported into Image J (NIH) for analysis. Morphometric measurements including mean linear intercept, average distal area space area and perimeter were quantified using previously described methods (12, 64). For alveolar attachment counts, alveolar attachments were identified and counted for each small airway and normalized to airway basement membrane length. For Gr-1 positive cell counts, 40x images of lung sections immunostained with an anti-Gr-1 antibody (MAB1037; R&D Systems) were captured and cell counts per high power field directly quantified. Smooth muscle actin immunostaining was done on lung sections using an anti-alpha smooth muscle actin antibody (ab5694; Abcam).
For pulmonary vessel density, lungs sections were immunostained with anti-vWF antibody (A0082; Dako) and vWF stained blood vessels < 50 μm in diameter were quantified per high power field.

RNA *in situ* hybridization and immunofluorescence imaging

RNAscope (ACD) was used to perform RNA *in situ* hybridization (RNA ISH) according to the manufacturer's instructions as previously described (63, 65). RNAscope probes to the following mouse genes were used for experiments – *Fbln5* (Cat# 493621, ACD) and *Eln* (Cat # 319361, ACD). Immunofluorescent images were then captured using an automated TiE inverted fluorescence microscope and a 100x Plain Apo objective (Nikon Instruments, Inc).

To identify proliferating parenchymal cells, lung sections were immunostained with anti-PCNA (2586; Cell Signaling Technology) and anti-pro-SPC (ab90716; Abcam) antibodies and imaged using a Keyence BZ-X710 fluorescent microscope with BZ-X viewer software (Keyence) with a 40X objective. Immunofluorescent images were then imported into image J for quantification of all PCNA positive cells (all proliferating cells) and pro-SPC /PCNA dual positive cells (proliferating type 2 alveolar epithelial cells) in the lung. Apoptotic cells were detected in formalin fixed paraffin-embedded lung sections using the *in situ* cell death detection kit (MilliporeSigma) as per the manufacturer's suggested methods.

Mouse lung fibroblast isolation and culture

Fibroblasts were isolated from PN5 and PN12 mouse lungs using previously described methods (12). Briefly, after perfusion with sterile phosphate-buffered saline, mouse lungs were harvested, dissected and enzymatically digested in Dulbecco's modified Eagle's medium (DMEM) containing collagenase type I (0.5mg/ml; Sigma-Aldrich) and collagenase type IA (0.5 mg/ml; Sigma-Aldrich), following by trituration to mechanically dissociate lung tissue. The resulting cell suspension was sequentially filtered through 100, 70 and 20 µm sterile filters. The filtrate from the 20-µm filter was plated in 100 mm cell-culture dishes and cultured in DMEM supplemented with 10% fetal calf serum. For all experiments, passage 3 or 4 fibroblasts were first plated in 12 or 24 well plates or chamber slides and cultured for 72 hours. After overnight

serum-starvation, cells were exposed to various treatment conditions for 4 – 48 hours in serum-free conditions prior to harvesting for RNA extraction or protein quantification.

Smad reporter assay

Saccular stage mouse lung fibroblasts were grown to 40-50% confluence in 24-well cell culture plates. Cells were transfected with 3 μg of SBE4-luc reporter, a luciferase reporter vector containing 4 copies of the Smad binding site (addgene) (66), and 0.3 μg of the Renilla luciferase control vector with Superfect transfection reagent (Qiagen) using the manufacturers suggested methods. Twenty four hours after tranfection, where appropriate, cells were treated with TGF-β1 (0.1 ng/ml) and/or HNE (1μg/ml) for 12 hours. Luminescence was then measured using the Dual Luciferase assay reagent on a GloMax plate reader (Promega).

Real-time quantitative PCR

Total RNA was extracted from neonatal lungs and lung fibroblasts using TRIzol reagent (Life Science Technologies) using standard methods (67). First strand cDNA was synthesized using oligo-dT primers and Moloney murine leukemia virus reverse transcriptase (Superscript II; Invitrogen). PCR primers were designed using PrimerQuest design tool (Integrated DNA Technologies). Two-step PCR was performed using an Applied Biosystems StepOne-Plus Real Time PCR system (Applied Biosystems) and SYBR Green detection system (Bio-Rad). Gene expression was normalized to β-actin in each sample. Fold change in mRNA expression was calculated using the 2^{-ddCT} method (68)

Western blot and densitometry

Mouse lung tissue and cultured lung fibroblasts were homogenized in radioimmunoprecipitation assay (RIPA) buffer with a protease and phosphatase inhibitor cocktail (Sigma-Aldrich). Total protein was quantified using a bicinchoninic acid protein assay kit

(Thermo Fisher Scientific). Equal amounts of protein from each sample was loaded on a NuPAGE polyacrylamide gel (Invitrogen) and transferred to a nitrocellulose membrane (Invitrogen). After blocking with Odyssey blocking buffer (LI-COR), membranes were sequentially incubated with primary and Odyssey IRDye 800CW and 680RD secondary antibodies. Primary antibodies used for western blot analysis were: anti-Phospho-Erk1/2 antibody (9101; Cell signaling Technology), anti-Total-Erk1/2 (9107; Cell signaling Technology) antibody and anti β-actin antibody (A5316; Sigma-Aldrich). Blots were detected using the Odyssey CLx imaging system (LI-COR). For densitometry analysis, TIFF images of blots were imported into Image J software (NIH) and quantified using standard methods.

Enzyme-linked immunosorbent assays

Mouse neutrophil elastase ELISA was done with kits purchased from R&D systems (Cat # MELA20). TGF-α ELISA were done using kits from MyBioSource (Cat # MBS2508394). All assays were done using the manufacturer's recommended methods. For all assays, samples were measured in duplicate. OD values were imported into Prism software (GraphPad), and concentrations determined and normalized to total protein content where indicated.

Human tracheal aspirate exosome isolation and quantification of elastase activity

Tracheal aspirates were collected from 11 BPD patients and 10 term-born control infants as previously described (21). Aspirate fluid was subjected to centrifugation at 10,000 G for 1 hour to pellet cells and smaller particles. Subsequently, the supernatant fluid was subjected to ultracentrifugation (150,000 G for 2 hours) for exosome extraction. Exosomes collected from individual patients within each group (BPD and control) were pooled, quantified and resuspended in PBS prior to use in experiments. Elastase content of exosome samples were measured in duplicate using the EnzChek Elastase assay kit (Molecular Probes, Grand Island,

NY) as per the manufacturer's suggested methods. Know concentrations of HNE were run in parallel to generate a standard curve. Exosome elastase activity was expressed in HNE equivalents.

Statistical analysis

All statistical analysis was done using Prism version 6.0 (GraphPad). Comparisons between groups were performed using a 2-tailed students t-test or a one-way analysis of variance followed by the Tukey post hoc test. $P < 0.05$ was used to determine statistical significance.

Study approval

The experiments in this study were conducted in accordance to the guidelines outlined by the US Public Health Service Policy on the Humane Care and Use of Laboratory Animals. All animal experimental protocols were approved by the IACUC at Vanderbilt University Medical Center (Protocol # M1700066). Collection of neonatal tracheal aspirates was performed with informed consent and approved by the Institutional review board at the University of Alabama at Birmingham (IRB-140926006).

Author Contributions

JTB, EJP, JMS, RVM, SD, SG, DSN, PMG, CSJ, WH, MX, PCD, AC, SK, DCN, BWR and JAK designed and performed experiments and analysed data. CVL, KD, AG and JEB provided the BPD and control patient exosomes. JTB, TSB, LRY and SHG conceived and designed the experiments. JTB and TSB drafted and revised the manuscript. All authors reviewed and approved the final manuscript.

Acknowledgements

Funding: This work is supported by NIH grants K12 HD087023 (Research Scholar, JTB), K08 HL133484 (JTB), K08 HL127102 (EJP), K12 HD087023 (Research Scholar, JMS), K08 HL143051 (JMS), K08 HL141652 (CVL), R01 HL119503 (LRY), K24HL143281 (LRY), R35 HL135710 (JEB), R01 GM108807 (SHG), P01 HL092870 (TSB); the Francis Family Foundation (JMS), American Heart Association grant AHA 17SDG32720009 (CVL); and US Department of Veteran Affairs grants IK2BX003841 (BWR), I01 BX002378 (TSB). Experiments were performed in part through the use of the Vanderbilt Cell Imaging Shared Resource (supported by NIH grants CA68485, DK20593, DK58404, DK59637 and EY08126) and the VMC Clow Cytometry Shared Resource (supported by the Vanderbilt Ingram Cancer Center - P30 CA68485 and the Vanderbilt Digestive Disease Research Center - DK058404)

References

1. Lange P, Celli B, Agusti A, Boje Jensen G, Divo M, Faner R, et al. Lung-Function Trajectories Leading to Chronic Obstructive Pulmonary Disease. *The New England journal of medicine.* 2015;373(2):111-22.
2. Martinez FD. Early-Life Origins of Chronic Obstructive Pulmonary Disease. *The New England journal of medicine.* 2016;375(9):871-8.
3. Postma DS, Bush A, and van den Berge M. Risk factors and early origins of chronic obstructive pulmonary disease. *Lancet.* 2015;385(9971):899-909.
4. Islam JY, Keller RL, Aschner JL, Hartert TV, and Moore PE. Understanding the Short- and Long-Term Respiratory Outcomes of Prematurity and Bronchopulmonary Dysplasia. *American journal of respiratory and critical care medicine.* 2015;192(2):134-56.
5. Doyle LW, Adams AM, Robertson C, Ranganathan S, Davis NM, Lee KJ, et al. Increasing airway obstruction from 8 to 18 years in extremely preterm/low-birthweight survivors born in the surfactant era. *Thorax.* 2016.
6. Baraldi E, Carraro S, and Filippone M. Bronchopulmonary dysplasia: definitions and long-term respiratory outcome. *Early human development.* 2009;85(10 Suppl):S1-3.
7. Kotecha SJ, Edwards MO, Watkins WJ, Henderson AJ, Paranjothy S, Dunstan FD, et al. Effect of preterm birth on later FEV1: a systematic review and meta-analysis. *Thorax.* 2013;68(8):760-6.
8. Wong PM, Lees AN, Louw J, Lee FY, French N, Gain K, et al. Emphysema in young adult survivors of moderate-to-severe bronchopulmonary dysplasia. *The European respiratory journal.* 2008;32(2):321-8.

9. Kallapur SG, and Jobe AH. Contribution of inflammation to lung injury and development. *Archives of disease in childhood Fetal and neonatal edition.* 2006;91(2):F132-5.

10. Watterberg KL, Demers LM, Scott SM, and Murphy S. Chorioamnionitis and early lung inflammation in infants in whom bronchopulmonary dysplasia develops. *Pediatrics.* 1996;97(2):210-5.

11. Van Marter LJ, Dammann O, Allred EN, Leviton A, Pagano M, Moore M, et al. Chorioamnionitis, mechanical ventilation, and postnatal sepsis as modulators of chronic lung disease in preterm infants. *The Journal of pediatrics.* 2002;140(2):171-6.

12. Benjamin JT, van der Meer R, Im AM, Plosa EJ, Zaynagetdinov R, Burman A, et al. Epithelial-Derived Inflammation Disrupts Elastin Assembly and Alters Saccular Stage Lung Development. *The American journal of pathology.* 2016;186(7):1786-800.

13. Cheng Ds, Han W, Chen SM, Sherrill TP, Chont M, Park GY, et al. Airway Epithelium Controls Lung Inflammation and Injury through the NF- B Pathway. *The Journal of Immunology.* 2007;178(10):6504-13.

14. Baraldo S, Turato G, and Saetta M. Pathophysiology of the small airways in chronic obstructive pulmonary disease. *Respiration.* 2012;84(2):89-97.

15. Shapiro SD, Endicott SK, Province MA, Pierce JA, and Campbell EJ. Marked longevity of human lung parenchymal elastic fibers deduced from prevalence of D-aspartate and nuclear weapons-related radiocarbon. *The Journal of clinical investigation.* 1991;87(5):1828-34.

16. Mariani TJ, Sandefur S, and Pierce RA. Elastin in lung development. *Experimental lung research.* 1997;23(2):131-45.

17. Abman SH. Bronchopulmonary dysplasia: "a vascular hypothesis". *American journal of respiratory and critical care medicine.* 2001;164(10 Pt 1):1755-6.

18. Bry K, Whitsett JA, and Lappalainen U. IL-1beta disrupts postnatal lung morphogenesis in the mouse. *American journal of respiratory cell and molecular biology.* 2007;36(1):32-42.

19. Speer CP. Inflammation and bronchopulmonary dysplasia: a continuing story. *Seminars in fetal & neonatal medicine.* 2006;11(5):354-62.

20. Merritt TA, Cochrane CG, Holcomb K, Bohl B, Hallman M, Strayer D, et al. Elastase and alpha 1-proteinase inhibitor activity in tracheal aspirates during respiratory distress syndrome. Role of inflammation in the pathogenesis of bronchopulmonary dysplasia. *The Journal of clinical investigation.* 1983;72(2):656-66.

21. Genschmer KR, Russell DW, Lal C, Szul T, Bratcher PE, Noerager BD, et al. Activated PMN Exosomes: Pathogenic Entities Causing Matrix Destruction and Disease in the Lung. *Cell.* 2019;176(1-2):113-26 e15.

22. Mihara K, Ramachandran R, Renaux B, Saifeddine M, and Hollenberg MD. Neutrophil elastase and proteinase-3 trigger G protein-biased signaling through proteinase-activated receptor-1 (PAR1). *The Journal of biological chemistry.* 2013;288(46):32979-90.

23. Zhao P, Lieu T, Barlow N, Sostegni S, Haerteis S, Korbmacher C, et al. Neutrophil Elastase Activates Protease-activated Receptor-2 (PAR2) and Transient Receptor Potential Vanilloid 4 (TRPV4) to Cause Inflammation and Pain. *The Journal of biological chemistry.* 2015;290(22):13875-87.

24. Kuang PP, Berk JL, Rishikof DC, Foster JA, Humphries DE, Ricupero DA, et al. NF-kappaB induced by IL-1beta inhibits elastin transcription and myofibroblast phenotype. *American journal of physiology Cell physiology.* 2002;283(1):C58-65.

25. Chen HC, Lin HC, Liu CY, Wang CH, Hwang T, Huang TT, et al. Neutrophil elastase induces IL-8 synthesis by lung epithelial cells via the mitogen-activated protein kinase pathway. *J Biomed Sci.* 2004;11(1):49-58.

26. Kohri K, Ueki IF, and Nadel JA. Neutrophil elastase induces mucin production by ligand-dependent epidermal growth factor receptor activation. *American journal of physiology Lung cellular and molecular physiology.* 2002;283(3):L531-40.

27. DiCamillo SJ, Carreras I, Panchenko MV, Stone PJ, Nugent MA, Foster JA, et al. Elastase-released epidermal growth factor recruits epidermal growth factor receptor and extracellular signal-regulated kinases to down-regulate tropoelastin mRNA in lung fibroblasts. *The Journal of biological chemistry.* 2002;277(21):18938-46.

28. DiCamillo SJ, Yang S, Panchenko MV, Toselli PA, Naggar EF, Rich CB, et al. Neutrophil elastase-initiated EGFR/MEK/ERK signaling counteracts stabilizing effect of autocrine TGF-beta on tropoelastin mRNA in lung fibroblasts. *American journal of physiology Lung cellular and molecular physiology.* 2006;291(2):L232-43.

29. Liu J, Rich CB, Buczek-Thomas JA, Nugent MA, Panchenko MP, and Foster JA. Heparin-binding EGF-like growth factor regulates elastin and FGF-2 expression in pulmonary fibroblasts. *American journal of physiology Lung cellular and molecular physiology.* 2003;285(5):L1106-15.

30. Kuang PP, Zhang XH, Rich CB, Foster JA, Subramanian M, and Goldstein RH. Activation of elastin transcription by transforming growth factor-beta in human lung

fibroblasts. *American journal of physiology Lung cellular and molecular physiology.* 2007;292(4):L944-52.

31. Stocks J, and Sonnappa S. Early life influences on the development of chronic obstructive pulmonary disease. *Ther Adv Respir Dis.* 2013;7(3):161-73.

32. McGrath-Morrow SA, and Collaco JM. Bronchopulmonary dysplasia: what are its links to COPD? *Ther Adv Respir Dis.* 2019;13:1753466619892492.

33. Vollsaeter M, Roksund OD, Eide GE, Markestad T, and Halvorsen T. Lung function after preterm birth: development from mid-childhood to adulthood. *Thorax.* 2013;68(8):767-76.

34. Bhandari A, and McGrath-Morrow S. Long-term pulmonary outcomes of patients with bronchopulmonary dysplasia. *Seminars in perinatology.* 2013;37(2):132-7.

35. Svanes C, Sunyer J, Plana E, Dharmage S, Heinrich J, Jarvis D, et al. Early life origins of chronic obstructive pulmonary disease. *Thorax.* 2010;65(1):14-20.

36. Bush A. Lung Development and Aging. *Annals of the American Thoracic Society.* 2016;13 Suppl 5:S438-S46.

37. Shapiro SD, Goldstein NM, Houghton AM, Kobayashi DK, Kelley D, and Belaaouaj A. Neutrophil elastase contributes to cigarette smoke-induced emphysema in mice. *The American journal of pathology.* 2003;163(6):2329-35.

38. Cavarra E, Martorana PA, Gambelli F, de Santi M, van Even P, and Lungarella G. Neutrophil recruitment into the lungs is associated with increased lung elastase burden, decreased lung elastin, and emphysema in alpha 1 proteinase inhibitor-deficient mice. *Laboratory investigation; a journal of technical methods and pathology.* 1996;75(2):273-80.

39. Nagai A, Yamawaki I, Takizawa T, and Thurlbeck WM. Alveolar attachments in emphysema of human lungs. *The American review of respiratory disease.* 1991;144(4):888-91.

40. Saetta M, Ghezzo H, Kim WD, King M, Angus GE, Wang NS, et al. Loss of alveolar attachments in smokers. A morphometric correlate of lung function impairment. *The American review of respiratory disease.* 1985;132(4):894-900.

41. Kim V, Rogers TJ, and Criner GJ. New concepts in the pathobiology of chronic obstructive pulmonary disease. *Proceedings of the American Thoracic Society.* 2008;5(4):478-85.

42. Grommes J, and Soehnlein O. Contribution of neutrophils to acute lung injury. *Mol Med.* 2011;17(3-4):293-307.

43. Aulakh GK. Neutrophils in the lung: "the first responders". *Cell and tissue research.* 2018;371(3):577-88.

44. Pierce MR, and Bancalari E. The role of inflammation in the pathogenesis of bronchopulmonary dysplasia. *Pediatric pulmonology.* 1995;19(6):371-8.

45. Auten RL, Jr., Mason SN, Tanaka DT, Welty-Wolf K, and Whorton MH. Anti-neutrophil chemokine preserves alveolar development in hyperoxia-exposed newborn rats. *American journal of physiology Lung cellular and molecular physiology.* 2001;281(2):L336-44.

46. Zaynagetdinov R, Sherrill TP, Gleaves LA, Hunt P, Han W, McLoed AG, et al. Chronic NF-kappaB activation links COPD and lung cancer through generation of an immunosuppressive microenvironment in the lungs. *Oncotarget.* 2016;7(5):5470-82.

47. Devaney JM, Greene CM, Taggart CC, Carroll TP, O'Neill SJ, and McElvaney NG. Neutrophil elastase up-regulates interleukin-8 via toll-like receptor 4. *FEBS Lett.* 2003;544(1-3):129-32.

48. Geraghty P, Rogan MP, Greene CM, Boxio RM, Poiriert T, O'Mahony M, et al. Neutrophil elastase up-regulates cathepsin B and matrix metalloprotease-2 expression. *J Immunol.* 2007;178(9):5871-8.

49. Domon H, Nagai K, Maekawa T, Oda M, Yonezawa D, Takeda W, et al. Neutrophil Elastase Subverts the Immune Response by Cleaving Toll-Like Receptors and Cytokines in Pneumococcal Pneumonia. *Front Immunol.* 2018;9:732.

50. Warburton D, Seth R, Shum L, Horcher PG, Hall FL, Werb Z, et al. Epigenetic role of epidermal growth factor expression and signalling in embryonic mouse lung morphogenesis. *Developmental biology.* 1992;149(1):123-33.

51. Alejandre Alcazar MA, Kaschwich M, Ertsey R, Preuss S, Milla C, Mujahid S, et al. Elafin Treatment Rescues EGFR-Klf4 Signaling and Lung Cell Survival in Ventilated Newborn Mice. *American journal of respiratory cell and molecular biology.* 2018;59(5):623-34.

52. Strandjord TP, Clark JG, Guralnick DE, and Madtes DK. Immunolocalization of transforming growth factor-alpha, epidermal growth factor (EGF), and EGF-receptor in normal and injured developing human lung. *Pediatric research.* 1995;38(6):851-6.

53. Stahlman MT, Orth DN, and Gray ME. Immunocytochemical localization of epidermal growth factor in the developing human respiratory system and in acute and chronic lung disease in the neonate. *Laboratory investigation; a journal of technical methods and pathology.* 1989;60(4):539-47.

54. Le Cras TD, Hardie WD, Deutsch GH, Albertine KH, Ikegami M, Whitsett JA, et al. Transient induction of TGF-alpha disrupts lung morphogenesis, causing pulmonary disease in adulthood. *American journal of physiology Lung cellular and molecular physiology.* 2004;287(4):L718-29.

55. Sproul EP, and Argraves WS. A cytokine axis regulates elastin formation and degradation. *Matrix biology : journal of the International Society for Matrix Biology.* 2013;32(2):86-94.

56. McGowan SE, and McNamer R. Transforming growth factor-beta increases elastin production by neonatal rat lung fibroblasts. *American journal of respiratory cell and molecular biology.* 1990;3(4):369-76.

57. Kotecha S, Wilson L, Wangoo A, Silverman M, and Shaw RJ. Increase in interleukin (IL)-1 beta and IL-6 in bronchoalveolar lavage fluid obtained from infants with chronic lung disease of prematurity. *Pediatric research.* 1996;40(2):250-6.

58. Rindfleisch MS, Hasday JD, Taciak V, Broderick K, and Viscardi RM. Potential role of interleukin-1 in the development of bronchopulmonary dysplasia. *J Interferon Cytokine Res.* 1996;16(5):365-73.

59. Liao J, Kapadia VS, Brown LS, Cheong N, Longoria C, Mija D, et al. The NLRP3 inflammasome is critically involved in the development of bronchopulmonary dysplasia. *Nat Commun.* 2015;6:8977.

60. Polosukhin VV, Degryse AL, Newcomb DC, Jones BR, Ware LB, Lee JW, et al. Intratracheal bleomycin causes airway remodeling and airflow obstruction in mice. *Experimental lung research.* 2012;38(3):135-46.

61. Lawson WE, Cheng DS, Degryse AL, Tanjore H, Polosukhin VV, Xu XC, et al. Endoplasmic reticulum stress enhances fibrotic remodeling in the lungs. *Proceedings of the National Academy of Sciences of the United States of America.* 2011;108(26):10562-7.

62. Alsafadi HN, Staab-Weijnitz CA, Lehmann M, Lindner M, Peschel B, Konigshoff M, et al. An ex vivo model to induce early fibrosis-like changes in human precision-cut lung slices. *American journal of physiology Lung cellular and molecular physiology.* 2017;312(6):L896-L902.

63. Sucre JMS, Vickers KC, Benjamin JT, Plosa EJ, Jetter CS, Cutrone A, et al. Hyperoxia Injury in the Developing Lung is Mediated by Mesenchymal Expression of Wnt5A. *American journal of respiratory and critical care medicine.* 2020.

64. Plosa EJ, Benjamin JT, Sucre JM, Gulleman PM, Gleaves LA, Han W, et al. beta1 Integrin regulates adult lung alveolar epithelial cell inflammation. *JCI Insight.* 2020;5(2).

65. Wang F, Flanagan J, Su N, Wang LC, Bui S, Nielson A, et al. RNAscope: a novel in situ RNA analysis platform for formalin-fixed, paraffin-embedded tissues. *J Mol Diagn.* 2012;14(1):22-9.

66. Zawel L, Dai JL, Buckhaults P, Zhou S, Kinzler KW, Vogelstein B, et al. Human Smad3 and Smad4 are sequence-specific transcription activators. *Mol Cell.* 1998;1(4):611-7.

67. Benjamin JT, Smith RJ, Halloran BA, Day TJ, Kelly DR, and Prince LS. FGF-10 is decreased in bronchopulmonary dysplasia and suppressed by Toll-like receptor activation. *American journal of physiology Lung cellular and molecular physiology.* 2007;292(2):L550-8.

68. Livak KJ, and Schmittgen TD. Analysis of relative gene expression data using real-time quantitative PCR and the 2(-Delta Delta C(T)) Method. *Methods.* 2001;25(4):402-8.

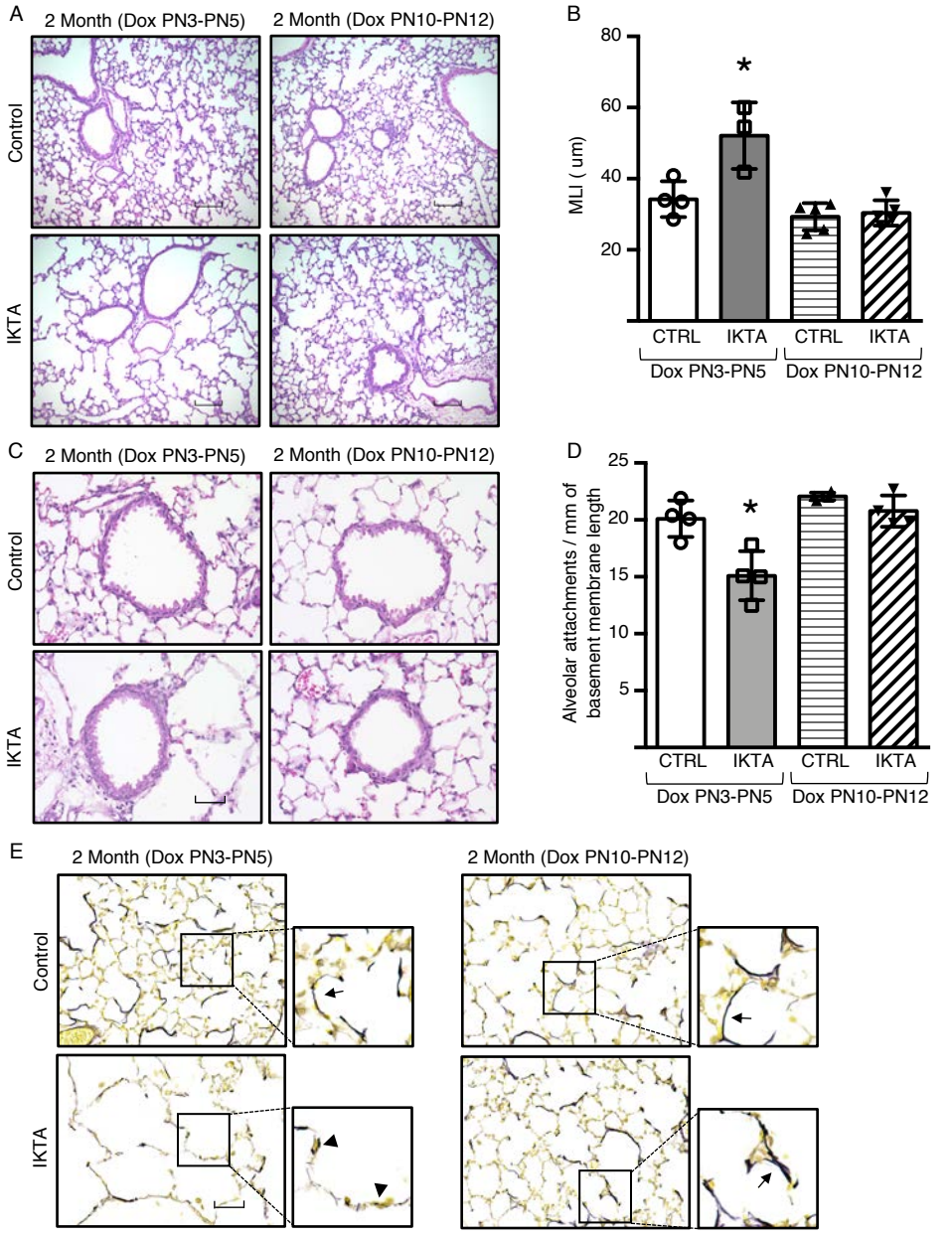

Figure 1. Epithelial NF-κB activation in saccular stage lungs results in emphysema, loss of alveolar attachments, and disruption of elastic fiber organization. Dams were treated with Dox from PN3–PN5 (saccular stage) or PN10-PN12 (alveolar stage), after which lungs from IKTA and litter-mate control mice were harvested at 2 months of age. (**A**) Representative hematoxylin and eosin staining and (**B**) morphometric evaluation of emphysema as measured by meal linear intercept (MLI). Data are expressed as mean ± SEM, n= 3-4 lungs per group, 5-6 imaged lung fields per lung, $*P < 0.05$ by one-way ANOVA and post-hoc Tukey test. (**C**) Representative H & E stained sections showing small airways (arrows denote alveolar attachments) and (**D**) alveolar attachment counts in control and IKTA lungs. Data are expressed as mean ± SEM, n= 3 lungs per group, $*P < 0.05$ by one-way ANOVA and post-hoc Tukey test. (**E**) Representative photomicrographs of Hart's elastin-stained lung sections. Arrows denote elastic fibers around airspaces. Arrowhead denotes fragmented elastic fibers. Scale bar: 100 μm in **A**, 50 μm in **C and E**.

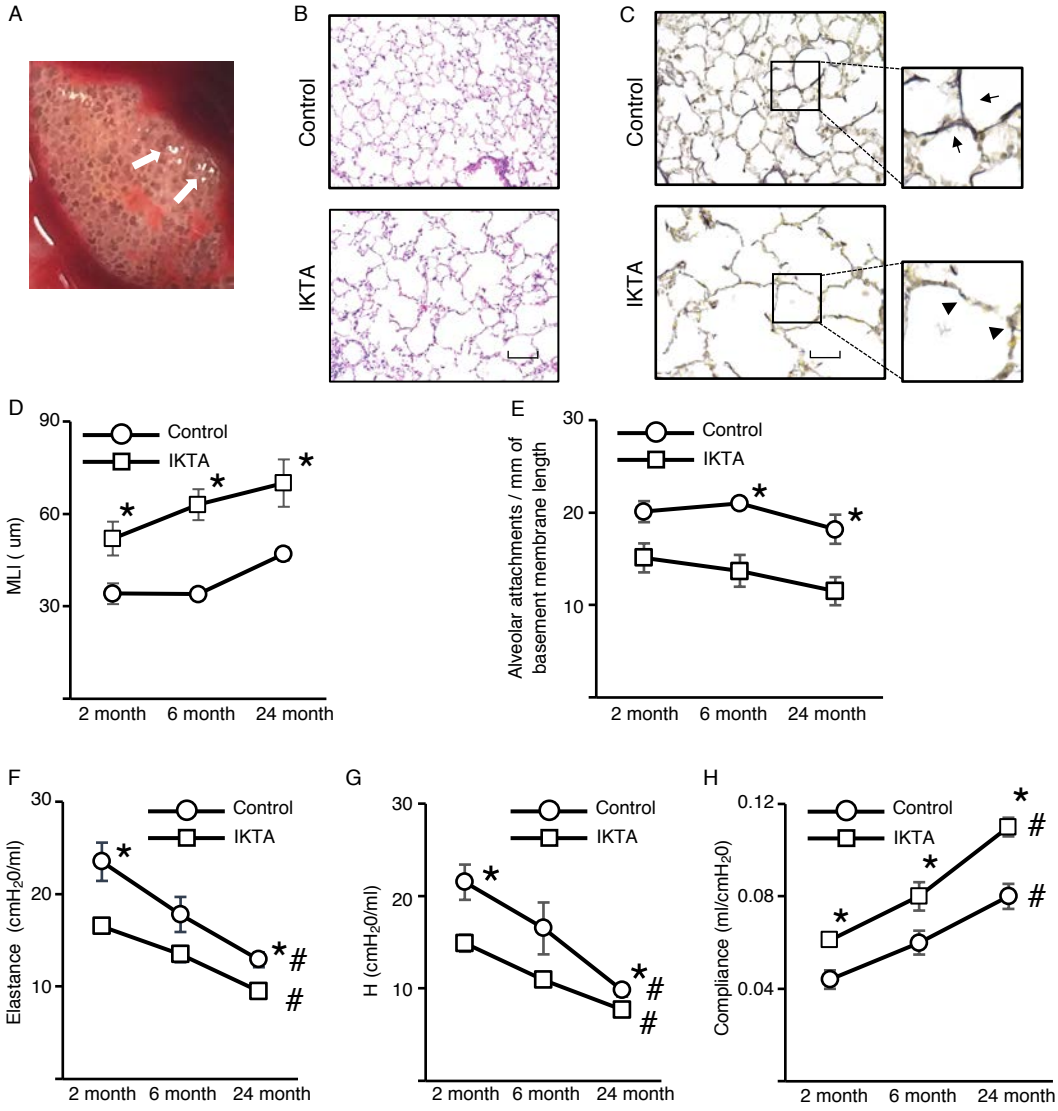

Figure 2. Epithelial NF-κB activation in saccular stage lungs results in lifelong abnormalities in lung structure and function. Dams were treated with Dox from PN3 – PN5 (saccular stage), after which lungs from IKTA and litter-mate control mice were harvested at 2, 6 or 24 months. (**A**) Representative image showing gross appearance of a 24-month IKTA lung. Arrows denote areas of emphysema. (**B** and **C**) Representative images showing H&E (**B**) and Hart's elastin stained (**C**) lung sections from 24-month control and IKTA lungs. Arrows denote intact elastic fibers. Arrowhead denotes fragments of elastic fibers. (**D** and **E**) Quantification of mean linear intercept (MLI) (**D**) and alveolar attachments (**E**) in control and IKTA lungs at 2,6 and 24 months. Data are expressed as mean ± SEM, n= 3-4 lungs per group, 6 imaged lung fields per lung, *$P < 0.05$ by 2-tailed Student's t-test comparing IKTA to litter-mate controls at each age. (**F** – **H**) Lung function, including total respiratory system elastance (**F**), tissue elastance (**G**), and dynamic compliance (**H**) was measured at 2,6 and 24 months in control and IKTA mice. Data are expressed as mean ± SEM, n= 4-6 mice per group, *$P < 0.05$ by 2-tailed Student's t-test comparing IKTA to litter-mate controls at each age, $^{\#}P < 0.05$ by one-way ANOVA and post-hoc linear trend test for each group (control and IKTA). Scale bar: 100 μm in **B**, 50 μm in **C**.

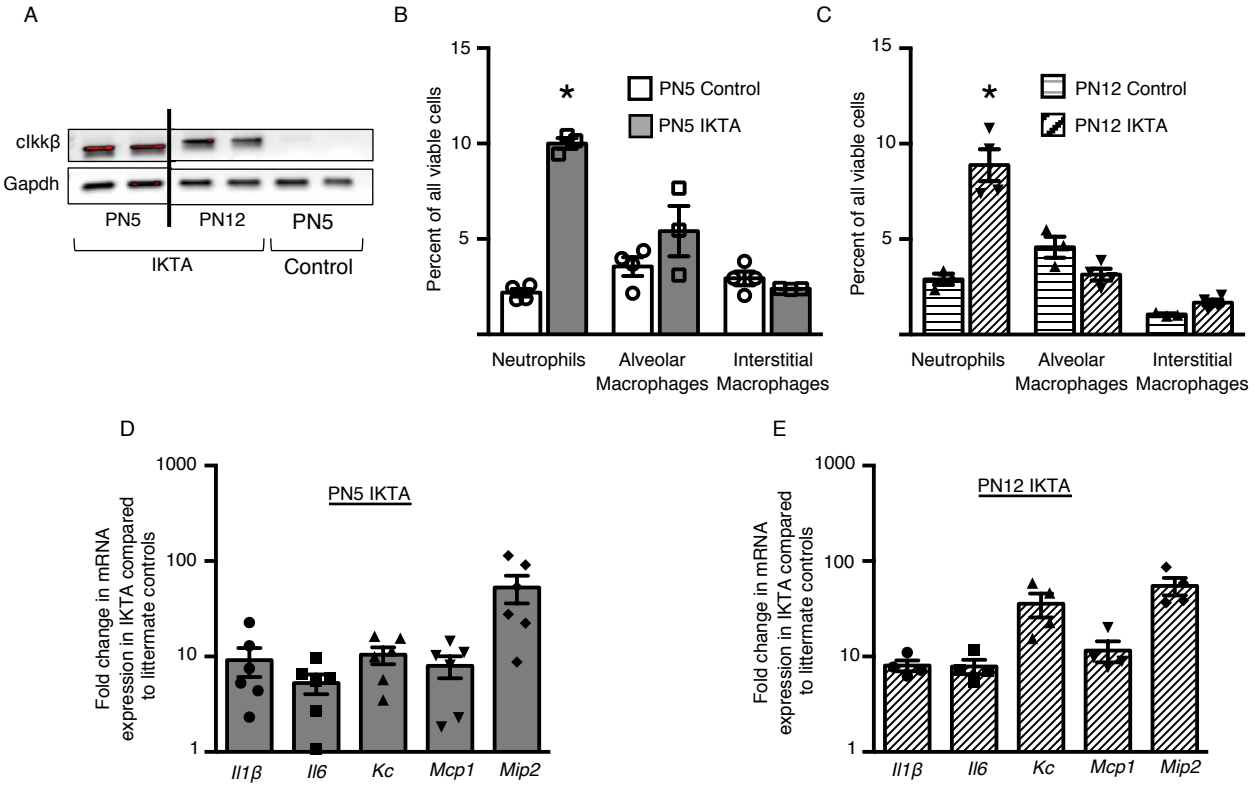

Figure 3. Transgene activation results in neutrophilic inflammation during both the saccular and alveolar stages of lung development. Dams were treated with Dox from PN3 – PN5 (saccular stage) or PN10 – PN12 (alveolar stage), after which lungs from IKTA and litter-mate control mice were harvested at PN5 or PN12. (**A**) Expression of constitutively active IKKβ (cIkkβ) transgene and gapdh was evaluated by PCR followed by agarose gel electrophoresis. (**B** and **C**) Quantification of immune cells in PN5 (**B**) and PN12 (**C**) control and IKTA lungs by flow cytometry. Data are expressed as mean ± SEM, n= 3-4 per group. ***P** < 0.05 by 2-tailed Student's *t* test. (**D** and **E**) mRNA expression of select inflammatory cytokines in PN5 (**D**) and PN12 (**E**) control and IKTA lungs. Data are expressed as mean ± SEM, n= 4-6 per group

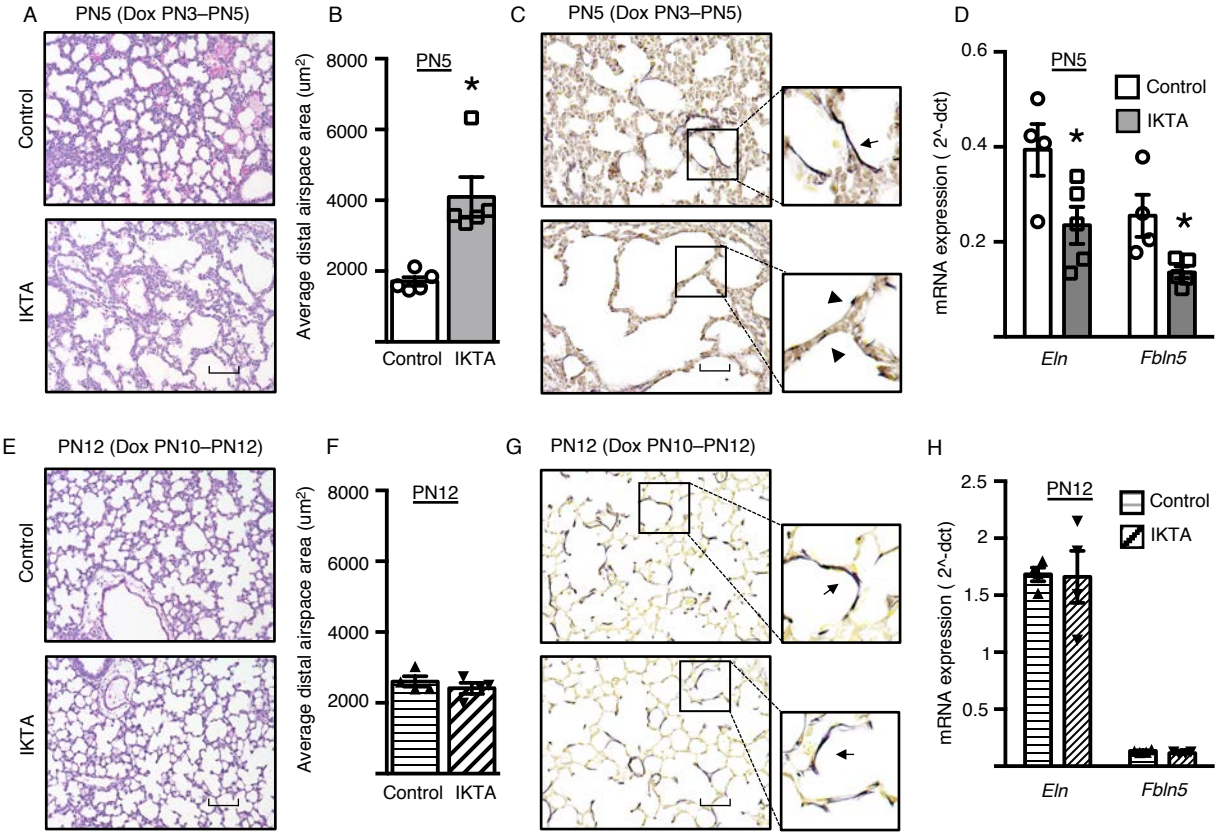

Figure 4. Neutrophilic inflammation disrupts saccular stage (but not alveolar stage) elastic fiber assembly and results in a BPD-like phenotype. Dams were treated with Dox from PN3 – PN5 (saccular stage) or PN10 – PN12 (alveolar stage), after which lungs from IKTA and litter-mate control mice were harvested at PN5 or PN12. (**A** – **B**) and (**E** – **F**) Representative hematoxylin and eosin stained lung sections (**A** and **E**) and morphometric measurements (**B** and **F**) demonstrated dilated terminal saccules in PN5 IKTA lungs while PN12 IKTA lungs appeared similar to controls. Data are expressed as mean ± SEM, n= 4-5 lungs per group, 5-6 imaged lung fields per lung, *$P < 0.05$ by 2-tailed Student's *t* test. (**C** and **G**) Representative photomicrographs of Hart's elastin-stained sections of PN5 (**C**) and PN12 (**G**) control and IKTA lungs demonstrating disorganized and fragmented elastic fibers in PN5 IKTA lungs. Arrows denote normal elastic fibers in controls. Arrowhead denotes fragmented elastic fibers in IKTA lungs. (**D** and **H**) mRNA expression of elastic fiber assembly components *Eln* and *Fbln5* expression in PN5 (**D**) and PN12 (**H**) IKTA lungs. Data are expressed as mean ± SEM, n=4-5 per group, *$P < 0.05$ by 2-tailed Student's *t* test. Scale bar: 100 μm in **A** and **E**, 50 μm in **C** and **G**.

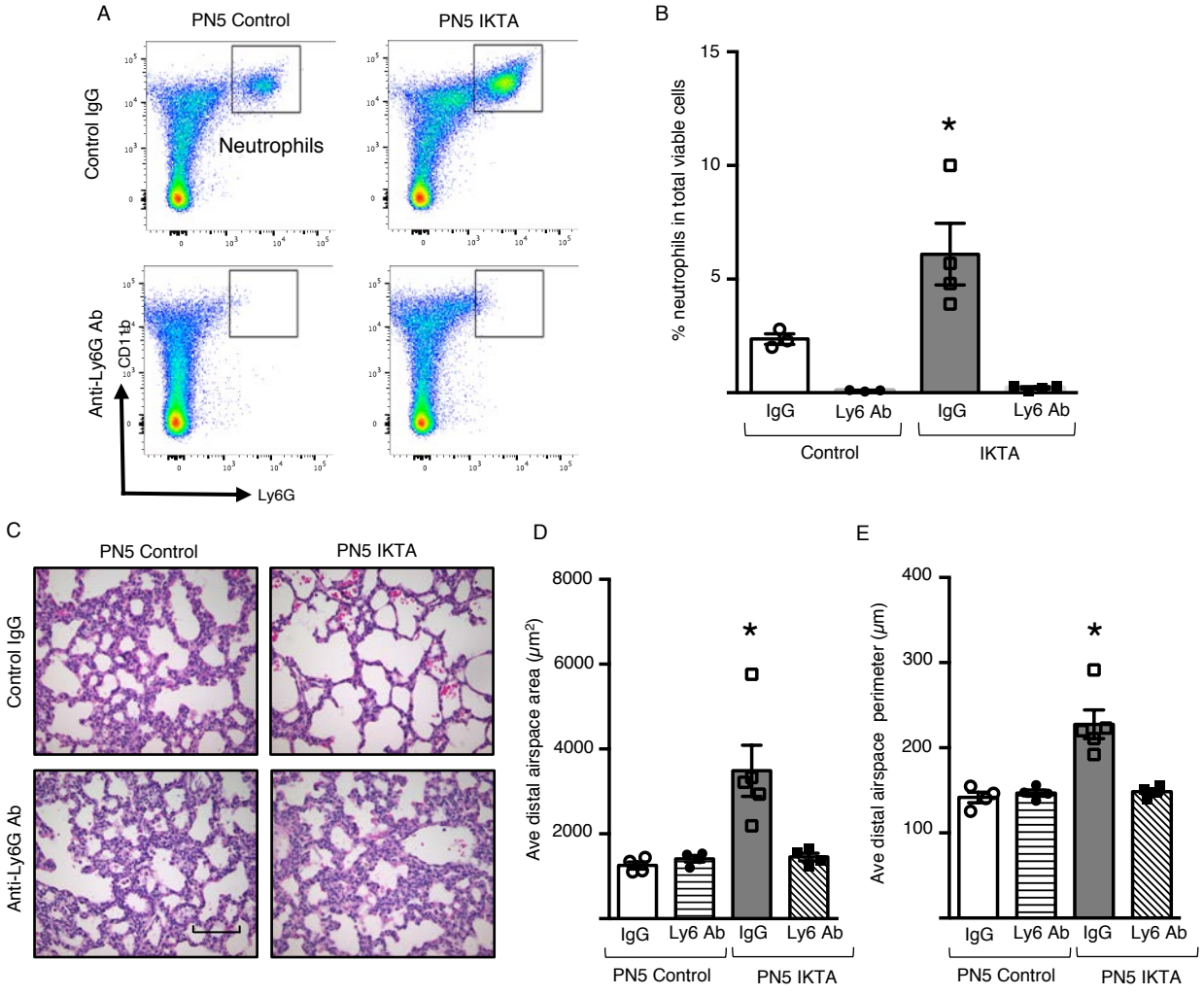

Figure 5. Neutrophil depletion rescues lung development in saccular stage lungs with NF-κB activation. Control and IKTA pups were administered anti-ly6G antibodies or control IgG by intraperitoneal injection on PN2 prior to placing dams on Dox from PN3-PN5 for transgene activation. (**A** and **B**) Representative flow plots (**A**) and quantification of $CD11b^{+}$ $Ly6G^{+}$ neutrophils (**B**) showing reduction in neutrophils with anti-ly6G antibody treatment. Data are expressed as mean ± SEM, n= 3-4 lungs per group, $*\boldsymbol{P} < 0.05$ by one-way ANOVA and post-hoc Tukey test. (**C** – **E**) Representative hematoxylin and eosin stained lung sections (**C**), morphometric evaluation of average distal airspace area (**D**), and average distal airspace perimeter (**E**) in PN5 lungs. Data are expressed as mean ± SEM, n= 4 lungs per group, 4-6 imaged fields per lung (**D** and **E**). $*\boldsymbol{P} < 0.05$ by one-way ANOVA and post-hoc Tukey test. Scale bar: 100 μm in **C**.

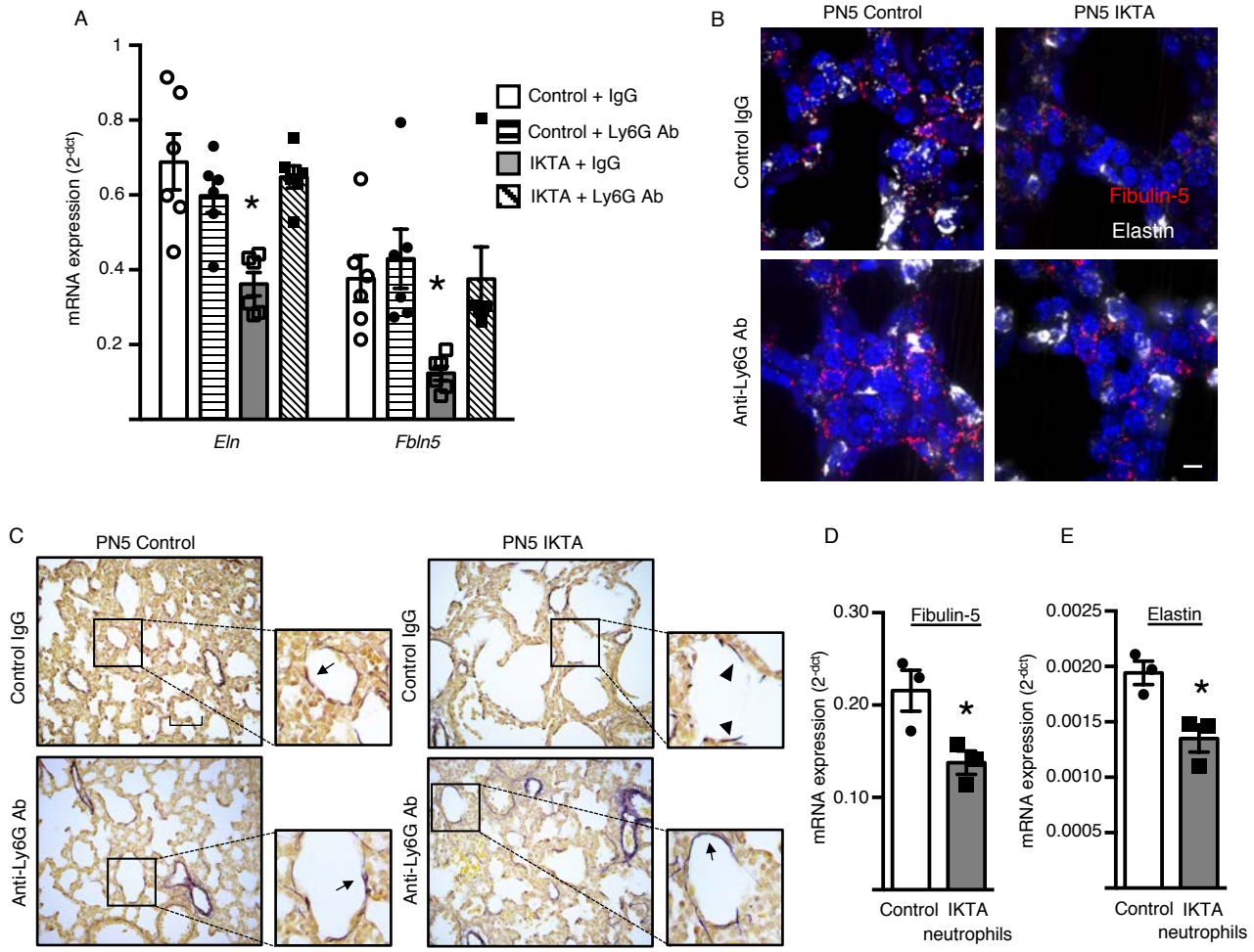

Figure 6. Neutrophil depletion prevents disruption of elastic fibers in saccular stage IKTA lungs. Control and IKTA pups were administered anti-ly6G antibodies or control IgG IP on PN2 prior to placing dams on Dox from PN3-PN5 for transgene activation. (**A**) Expression of *Eln* and *Fbln5* in PN5 lungs. Data are expressed as mean ± SEM, n=6 per group, ****P*** < 0.05 by one-way ANOVA and post-hoc Tukey test. (**B**) Representative photomicrographs of RNAscope-labelled sections from PN5 lungs. *Fbln5* and *Eln* expressing cells were reduced in IKTA lungs with control IgG treatment, but *Fbln5* and *Eln* expression appeared similar to controls in IKTA mice with anti-Ly6G antibody treatment. (**C**) Representative Hart's elastin-stained sections from PN5 lungs showing normal cord-like structures around airspaces in IKTA mice treated with anti-Ly6G antibodies. Arrows denote elastic fibers around airspaces. Arrowhead denotes fragmented elastic fibers. (**D** and **E**) $CD11b^+$ $Ly6G^+$ neutrophils were isolated from IKTA lungs and co-cultured with wild-type saccular stage lung fibroblast for 4 hours. Expression of *Fbln5* (**D**) and *Eln* (**E**) was reduced in saccular stage lung fibroblasts cocultured with IKTA neutrophils. Data are expressed as mean ± SEM, n=3 per group. Data are representative of 3 independent experiments. (**D** and **E**), ****P*** < 0.05 by 2-tailed Student's *t* test. Scale bar: 10 μm in **B,** 50 μm in **C**.

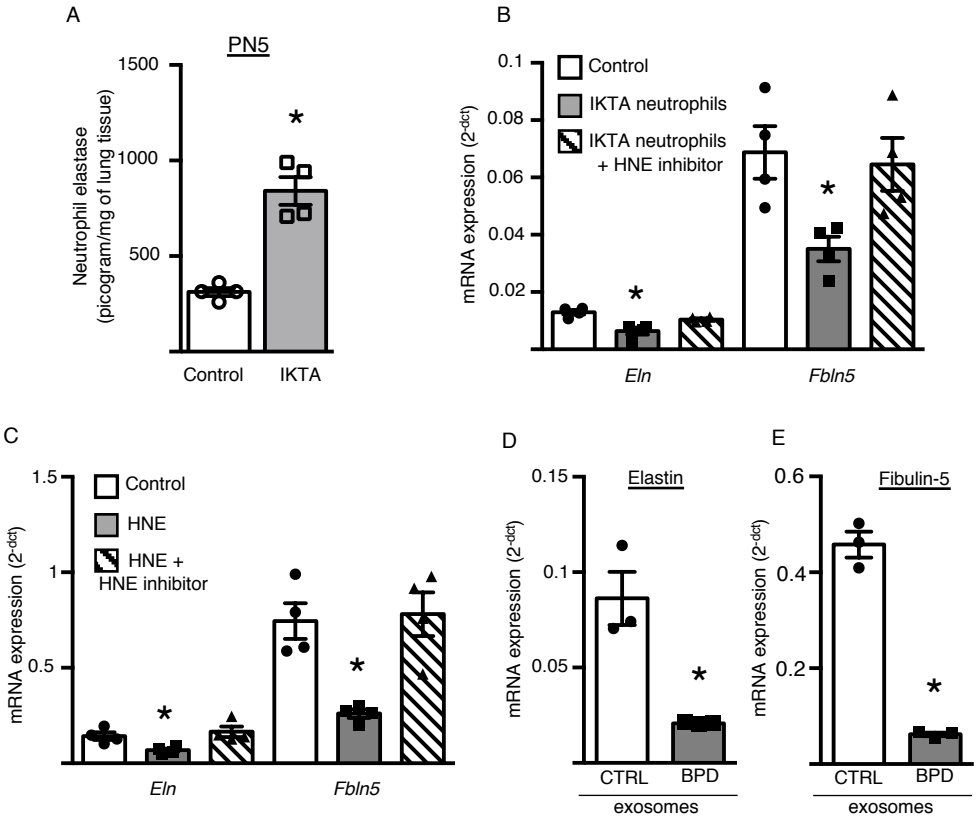

Figure 7. Neutrophil elastase inhibits expression of elastic fiber assembly components by saccular stage mouse lung fibroblasts. (**A**) Quantification of neutrophil elastase (NE) by ELISA in PN5 control and IKTA lung homogenates. Data are expressed as mean ± SEM, n=4-6 per group, ***P** < 0.05 by 2-tailed Student's t-test. (**B** and **C**) PN5 mouse lung fibroblasts were cultured with or without IKTA neutrophils for 4 hours (**B**) or purified human neutrophil elastase (HNE) 1 μg/ml for 24 hours (**C**) and *Eln* and *Fbln5* expression was quantified. Where indicated, cells were also pretreated with 10μM N-Methoxysuccinyl-Ala-Ala-Pro-Val-chloromethyl ketone (HNE inhibitor). Data expressed as mean ± SEM, n= 4 per group. Data are representative of 4 independent experiments. ***P** < 0.05 compared to control by one-way ANOVA and post-hoc Tukey test. (**D** and **E**) Saccular stage mouse lung fibroblasts were cultured with tracheal aspirate exosomes (10^9 exosomes/ml) isolated from preterm infants with severe BPD (BPD) or from term-born control infants (CTRL) and *Eln* (**D**) and *Fbln5* (**E**) expression was quantified. Data are expressed as mean ± SEM, n= 3 per group, ***P** < 0.05 by 2-tailed Student's t-test.

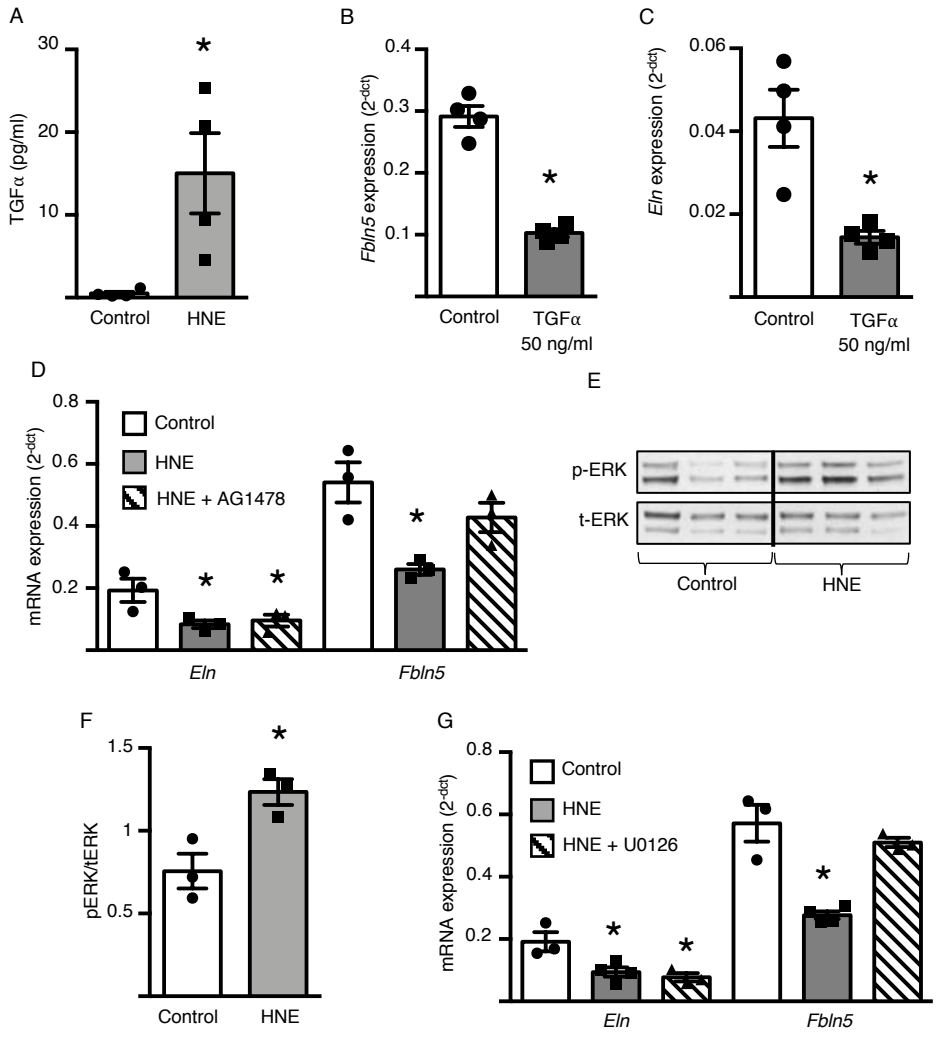

Figure 8. Neutrophil elastase downregulates mRNA expression of fibulin-5 in saccular stage mouse lung fibroblasts through EGFR-MEK-ERK signaling. PN5 mouse lung fibroblasts were grown to confluence and cultured with or without purified human neutrophil elastase (HNE) at 1 or 4 μg/ml or TGFα (50 ng/ml) for up to 24 hours. In some experiments, fibroblasts were treated with AG1479 10μM (EGFR inhibitor) or U0126 25 μM (MEK inhibitor) prior to HNE treatment. (**A**) TGFα ELISA from conditioned media samples after 15 minutes of HNE treatment of saccular stage lung fibroblasts. Data are expressed as mean ± SEM, n=4 per group. (**B** and **C**) Quantification of *Fbln5* (**B**) and *Eln* (**C**) expression by qPCR in saccular stage fibroblasts 24 hours after treatment with TGFα. Data are expressed as mean ± SEM, n=4 per group. (**D**) Expression of *Eln* and *Fbln5* in fibroblasts treated with HNE ± AG1479 10μM for 24 hours. Data are expressed as mean ± SEM, n=3-4 per group. (**E** and **F**) Western blot analysis of phospho-Erk1/2 and total-Erk1/2 in cell lysates from fibroblasts treated with HNE for 15 minutes. Data are expressed as mean ± SEM, n=3 per group. (**G**) Expression of *Eln* and *Fbln5* in fibroblasts treated with HNE ± U0126 10μM for 24 hours. Data are expressed as mean ± SEM, n=3-4 per group. Data are representative of 3 independent experiments. ***P** < 0.05 compared to control by 2-tailed student's t-test (**A,B,C** and **F**); ***P** < 0.05 compared to control by one-way ANOVA and post-hoc Tukey test (**D** and **G**).

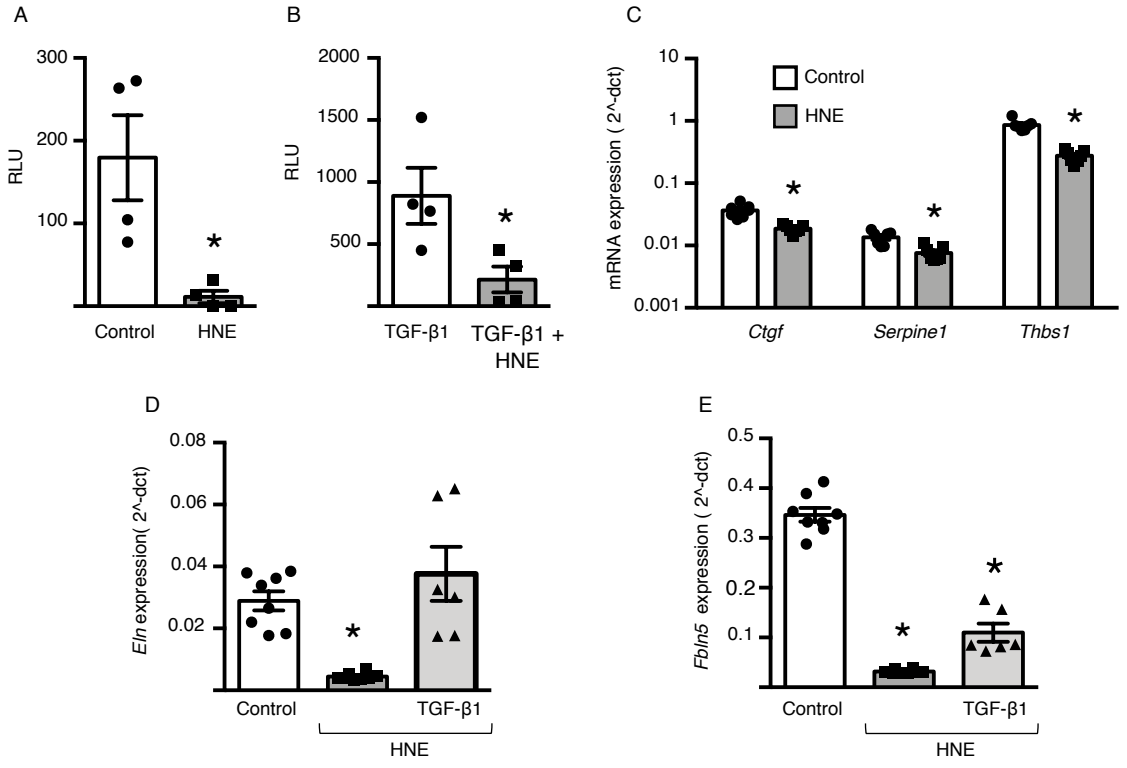

Figure 9. Neutrophil elastase downregulates TGF-β signaling and reduces elastin expression in saccular stage lung fibroblasts. (**A** and **B**) PN5 mouse lung fibroblasts were transfected with a Smad luciferase reporter (SBE4-Luc) and treated with or without HNE (1μg/ml) and/or recombinant TGF-β1 (0.1 ng/ml) for 12 hours. Luminescence measurements are reported as relative light units (RLU) above background (untransfected control) in (**A**) Control cells and (**B**) TGF-β1 treated cells. Data are expressed as mean ± SEM, n=4 per group. *$\boldsymbol{P} < 0.05$ by 2-tailed Student's t-test. (**C** – **E**) Mouse lung fibroblasts were cultured with or without HNE (1μg/ml) and TGF-β1(0.1 ng/ml) for 24 hours. (**C**) mRNA expression of *Ctgf, Serpine1* and *Thbs1* in fibroblasts treated with or without HNE. Data are from 3 independent experiments and expressed as mean ± SEM, n=7 per group. * $^{\#}\boldsymbol{P} < 0.05$ by 2-tailed Student's t-test. (**D** and **E**) mRNA expression of *Eln* (**D**) and *Fbln5* (**E**) in saccular stage fibroblasts treated with HNE ± recombinant TGF-β1. Data are from 3 independent experiments and expressed as mean ± SEM, n=6-8 per group, *$\boldsymbol{P} < 0.05$ compared to control by one-way ANOVA and post-hoc Tukey test.